

Cathode diameter and operating parameter effects on hafnium cathode evaporation for oxygen plasma cutting arc

メタデータ	言語: English 出版者: 公開日: 2017-10-03 キーワード: 作成者: Long, Nguyen Phi, Tanaka, Yasunori, Uesugi, Yoshihiko メールアドレス: 所属:
URL	http://hdl.handle.net/2297/32843

Numerical investigation of the effect of cathode holder shape on hafnium cathode evaporation for oxygen plasma cutting arc

Nguyen Phi Long^{1,2}, Yasunori Tanaka¹, and Yoshihiko Uesugi¹

¹ Division of Electrical Engineering and Computer Science, Kanazawa University, Kakuma, Kanazawa 920-1192, Japan

E-mail: de102102@ec.t.kanazawa-u.ac.jp

Abstract. The effects of cathode holder shape on a plasma cutting arc are investigated using a 2-D thermofluid model developed for arc plasma with consideration of hafnium cathode evaporation. The cathode holder shape is defined a convex structure which protrudes from the surface of the cathode holder. Results show that the gas flow near the hafnium cathode is attracted towards to cathode with effect of convex cathode holder. The temperature of cathode surface decreases markedly with the higher protrusion of convex cathode holder by a rapid clockwise rotation of gas flow velocity. The presence of gas flow vortex toward to cathode surface reduces the mass fraction of hafnium vapor on surface cathode. Thus, the amount of mass loss of hafnium evaporation was predicted to decreases significantly with effect of convex cathode holder.

Submitted to: *J. Phys. D: Appl. Phys.*

² Author to whom any correspondence should be addressed.

1. Introduction

The plasma arc cutting process is a technique widely used for cutting different metals with high-speed and high-accuracy in the industrial fields. An arc plasma is established between the electrode in the plasma torch and a work-piece. Cathode erosion in plasma arc cutting is a process that still introduces a limit on performance improvement when using hafnium cathode and oxygen gas plasma. It is necessary to understand in detail of interactions between the electrode and the arc plasma as well as the arc cathode erosion on performance improvement and lifetime of plasma arc cutting devices.

A summary of research related to plasma arc cutting processes can be found in a topical review [1, 2]. During operation of plasma arc cutting torch, the molten material is ejected from surface of cathode insert [3]. A significant amount of the material deposits on the inside surface of the nozzle and also change the geometry of the cathode. Thus, the shape of surface of insert changes rapidly until reaching the preferred concave shape at steady state [4]. As for the cathode with concave surface insert used in plasma arc torch, it has been shown in patent literature [4, 5] that the curvature of this preferred concave shape is function of the current level of the torch, the diameter of the insert and the gas flow pattern in the torch. Using this insert shape that provides for reduced deposition of the high thermionic emissivity material on the nozzle, thereby reducing nozzle wear in the torch. The results of report [6] suggested that the plasma temperature is decreased by heavy deposits of eroded cathode material on nozzle after the large crater forms in cathode, and the cut quality also decreases in case of cathode pit wears. The authors of the reports [7, 8] suggested a start-up erosion mechanism by using high-speed camera imaging. A comparison of the behaviour during the start-up phases of new or used electrodes has investigated with different emission surface. The new ones, both with or without the initially shaped emission surface, are characterized by a quite short transient towards stabilization of the arc column at the centre of the Hf surface with a smooth transition event without massive ejection of melted Hf-based particles. In contrast, the used electrodes are characterized by a quite long transient phase with the ejection of molten particles.

In addition, multiple reports of studies investigating the process parameters related to plasma arc cutting have been published. [9]–[13]. Nemchinsky [9] confirmed that swirling the gas enhances the gas flow from the cathode. This enhanced flow sweeps the evaporated particles away from the cathode and thus increases the net evaporation rate. Another experimental result indicated the importance of the flow pattern close to the cathode [1, 10]: the erosion rate decreases with time for long arc duration tests. There exists a stagnation zone inside this crater. Slowing down of the gas flow increases the probability of the evaporated atom/ion returning to the cathode and thus decreases the net erosion rate. Our previous works [12, 13] have already used a numerical model for a fundamental study of effect of various swirl gas angle and process parameters on behaviour of hafnium cathode evaporation on plasma cutting arc torch. Results have shown that a larger swirl gas angle causes a high-temperature plasma area in front of

the cathode surface shrunken in a radial direction. The flow patterns changed to the opposite direction in front of the cathode and induced hafnium vapor transportation along the center axis direction at a large swirl angle.

As discussed above, the geometry of electrode has a marked effect on the characteristics of arc plasma. It is complicated to investigate the interaction between thermal plasma and surface cathode insert shape such as evaporation of the cathode material by numerical calculation. In addition, the experiment calculations of arc plasma torch with shape of hafnium cathode insert are very difficult by high cost of hafnium material. However, another approach for geometry of electrode is investigated the shape of cathode holder. This holder structure may affect the characteristics of arc plasma, especially gas flow pattern and amount of ejected cathode material. Numerical modeling is extremely important to predict the erosion amount of hafnium cathode holder geometry in plasma cutting arcs to enhance the performance and the lifetime of plasma arc cutting devices.

The aim of this work is to investigate the effects of cathode holder shape on hafnium cathode evaporation by a developed numerical model for oxygen plasma cutting. The cathode holder shape is defined a convex structure which protrudes from the surface of the cathode holder. The governing equations for mass, momentum, and energy transfer from the evaporated material to the arc plasma are used to obtain the simulation results which have been setup in the previous work [12, 13]. This developed model incorporates evaporation phenomena of the hafnium cathode and the re-deposition of hafnium vapour on the cathode surface [9]. Using this model, the temperature field, gas flow pattern, and mass fraction of hafnium vapour inside of plasma cutting torch as well as the total amount of mass loss of the hafnium cathode caused by evaporation were obtained with shape of cathode holder.

2. Mathematical model

2.1. Calculation model and assumptions

Figure 1 portrays a schematic diagram of the arc model and the calculation space of the DC plasma cutting arc torch used in this work. The copper electrode has a hafnium tip insert of 1.27 mm in diameter. Oxygen, which is the plasma gas used for these experiments, is supplied from the inlet by swirling gas flow. The distance between the cathode surface and nozzle bore exit is approximately 8 mm. The arc plasma is constricted by the copper nozzle. The nozzle outlet has 1.33 mm in diameter. Calculations were performed in the $r - z$ two-dimensional cylindrical coordinate system.

As described in this paper, the developed two-dimensional numerical modeling assumes the following. The gas flow is laminar. The plasma is in a steady state and axisymmetric. For simplicity in modeling, the thermal plasma is under local thermal equilibrium (LTE) conditions, which means the electron and heavy-particle temperatures are equal. The arc is assumed to be optically thin with radiative energy

losses. The effect of swirl gas flow is considered. A simple energy balance equation is set up at the cathode surface to determine the hafnium evaporation process and to calculate the mass loss of hafnium evaporation. The electric field has only an axial component, whereas the magnetic field has only an azimuthal component. The evaporation amount of the hafnium cathode was predicted considering the evaporation flux estimated using the saturation vapour pressure and the re-deposition flux. The arc radiation was estimated according to the net emission coefficient as described later.

2.2. Governing equations for gas and plasma

Based on the assumptions described above, the gas and arc plasma are governed by the following equations:

- Mass conservation:

$$\nabla \cdot (\rho \mathbf{u}) = S_p^{\text{Hf}} \quad (1)$$

- Momentum conservation:

Axial:

$$\begin{aligned} \nabla \cdot (\rho \mathbf{u} \mathbf{u}) &= -\frac{\partial p}{\partial z} + \nabla \cdot (\eta \nabla u) + \nabla \cdot \left(\eta \frac{\partial \mathbf{u}}{\partial z} \right) \\ &\quad - \frac{2}{3} \frac{\partial}{\partial z} (\eta \nabla \cdot \mathbf{u}) \end{aligned} \quad (2)$$

Radial:

$$\begin{aligned} \nabla \cdot (\rho \mathbf{u} \mathbf{v}) &= -\frac{\partial p}{\partial r} + \nabla \cdot (\eta \nabla v) + \nabla \cdot \left(\eta \frac{\partial \mathbf{u}}{\partial r} \right) \\ &\quad - 2\eta \frac{v}{r^2} + \frac{\rho w^2}{r} - \frac{2}{3} \frac{\partial}{\partial r} (\eta \nabla \cdot \mathbf{u}) - \mu_0 \sigma E_z H_\theta \end{aligned} \quad (3)$$

Swirl:

$$\nabla \cdot (\rho \mathbf{u} \mathbf{w}) = \nabla \cdot (\eta \nabla w) - \frac{\rho v w}{r} - \frac{\rho w}{r^2} \frac{\partial}{\partial r} (r \eta) \quad (4)$$

- Energy conservation:

$$\begin{aligned} \nabla \cdot (\rho \mathbf{u} h) &= \nabla \cdot \left(\frac{\lambda}{C_P} \nabla h \right) + \mathbf{u} \cdot \nabla p + \sigma |E_z|^2 \\ &\quad - P_{\text{rad}} - L_v S_p^{\text{Hf}} \end{aligned} \quad (5)$$

- Mass conservation for Hf vapour:

$$\nabla \cdot (\rho \mathbf{u} Y_{\text{Hf}}) = \nabla \cdot (\rho D_{\text{Hf-O}_2} \nabla Y_{\text{Hf}}) + S_p^{\text{Hf}} \quad (6)$$

- Ohm's law:

$$E_z = \frac{I}{\int 2\pi r \sigma dr} \quad (7)$$

- Ampere's law:

$$H_\theta = \frac{1}{r} \int_0^r \sigma E_z \xi d\xi \quad (8)$$

In those equations, \mathbf{u} is the gas flow vector; r and z respectively denote the radial and axial positions. Additionally, u , v , and w respectively represent the axial, radial, and swirl gas flow velocities. The following are other important variables: ρ , mass density; h , enthalpy; p , pressure; η , viscosity; σ , electrical conductivity; λ , thermal conductivity; C_p , specific heat at constant pressure; P_{rad} , radiation loss; ξ , radial coordinate; E_z , electric field in axial direction; H_θ , magnetic field in azimuthal direction; Y_{Hf} , mass fraction of Hf vapour; $D_{\text{Hf-O}_2}$, effective diffusion coefficient of Hf vapour in O_2 ; L_v , latent heat for evaporation; S_p^{Hf} , the mass production rate because of evaporation; and I , the total electric current. In the equation of (5), we neglected gradient term of electron enthalpy for simplicity.

2.3. Governing equations for electrodes

Inside the solid and liquid, the energy conservation equation is established as

$$0 = \frac{\partial}{\partial z} \left(\frac{\lambda_s}{C_{\text{ps}}} \frac{\partial h_s}{\partial z} \right) + \frac{1}{r} \frac{\partial}{\partial r} \left(r \frac{\lambda_s}{C_{\text{ps}}} \frac{\partial h_s}{\partial z} \right) + \sigma_s |E_z|^2, \quad (9)$$

where h_s signifies the enthalpy of the solid/liquid, C_{ps} denotes the specific heat of the solid/liquid, λ_s stands for the thermal conductivity of the solid/liquid, and σ_s represents the electrical conductivity of the solid/liquid. The enthalpy of the solid is related to specific heat as shown below.

$$h_s(T_s) = \int_{T_0}^{T_s} C_{\text{ps}}^{\text{eff}} dT_s \quad (10)$$

$$C_{\text{ps}}^{\text{eff}} = \begin{cases} \frac{L_m}{\Delta T} & (T_{\text{melt}} - \Delta T \leq T_s \leq T_{\text{melt}}) \\ C_{\text{ps}} & (\text{otherwise}) \end{cases} \quad (11)$$

Therein, the following variables are used: T_s , temperature of the solid/liquid; T_0 , reference temperature ($T_0=300$ K); T_{melt} , melting temperature; $C_{\text{ps}}^{\text{eff}}$, effective specific heat; L_m , latent heat for melting of solid; and ΔT , step temperature for melting ($\Delta T=5$ K).

In this model, interaction between the thermal plasma and solid is solved. Heat transfer to the surface cathode in this model can occur through the thermal energy of ions, heating by surface recombination of ions and energy loss by electron emission, and thermal conduction from the arc plasma and thermal radiation from the cathode. The heating of cathode by radiation from the arc can be neglected in comparison with the other energy fluxes for a simplified model. These are described by the following additional heat flux to the energy conservation equation for the cathode surface:

$$q_K = \frac{j_{\text{ion}}}{e} \left(\frac{3}{2} k T_p + \epsilon_{\text{ion}} - W_\ell \right) - \frac{j_e}{e} W_\ell - \frac{\lambda_{\text{pc}}}{\Delta z} (T_c - T_p) - \delta_\ell \sigma_{\text{sb}} (T_c^4 - T_a^4). \quad (12)$$

The current density, because of thermionic emission, depends on the cathode temperature using the well-known Richardson–Dushman equation with the Schottky

effect, which is given as presented below.

$$j_e = \alpha_\ell A T_c^2 \exp\left(-\frac{W_\ell}{kT_c}\right) \exp\left(-\frac{e}{2kT_c} \sqrt{\frac{eE_0}{\pi\epsilon_0}}\right) \quad (13)$$

$$j_{\text{ion}} = \max(0, \sigma E_0 - j_e) \quad (14)$$

In those equations, the following variables are used: q_K , heat flux between the surface cathode and plasma; T_p , temperature of the plasma contacting with the cathode; T_c , temperature of the surface cathode contacting with the plasma; T_a , ambient temperature, here 300 K as the wall temperature of nozzle; e , elementary charge; k , Boltzmann's constant; σ_{sb} , Stefan–Boltzmann's constant; A , thermionic emission constant; ϵ_0 , vacuum permittivity; W_ℓ , work function of Hf and Cu; ϵ_{ion} , ionization energy of oxygen ion; δ_ℓ , solid emissivity; (assumed to be 0.3); α_ℓ , material factor for thermionic emission; j_e , thermionic emission current density of electron; j_{ion} , ion current density; E_0 , electric field at the cathode surface; λ_{pc} , thermal conductivity of cathode; and Δz , distance between the surface cathode and the center of the control volume. The present calculation neglected the radial components of current density, electric field.

2.4. Governing equations for evaporation flux

The mass production rate attributable to evaporation S_p^{Hf} is calculable approximately as

$$S_p^{\text{Hf}} = \begin{cases} m_{\text{Hf}}(\Gamma_{\text{evp}} - \Gamma_{\text{dep}}) \frac{\Delta S}{\Delta V} & (\text{neighbor to wall}) \\ 0 & (\text{otherwise}) \end{cases} \quad (15)$$

Therein, m_{Hf} is the effective mass of Hf vapour, Γ_{evp} is the mass flux of evaporated vapour, Γ_{dep} is the mass flux of re-deposition, ΔS is the surface of evaporated Hf, and ΔV is the volume of the control volume.

The mass flux of the evaporated vapour Γ_{evp} was calculated using the following Hertz–Knudsen relation, as

$$m_{\text{Hf}} \Gamma_{\text{evp}} = m_{\text{Hf}} \frac{1}{4} \frac{P_v}{kT_c} \sqrt{\frac{8kT_c}{\pi m_{\text{Hf}}}} = P_v \sqrt{\frac{m_{\text{Hf}}}{2\pi kT_c}}, \quad (16)$$

where P_v is the saturation vapour pressure of hafnium vapour.

The saturation vapour pressure P_v was evaluated using the Clausius–Clapeyron relation as

$$P_v = \begin{cases} P_{\text{1atm}} \exp\left[\frac{L_v}{R_{\text{Hf}}}\left(\frac{1}{T_{\text{boil}}} - \frac{1}{T_c}\right)\right] & (T_c \geq T_{\text{melt}}) \\ P_{\text{melt}} \frac{T_c - T_{\text{melt}} + \Delta T}{\Delta T} & (T_c < T_{\text{melt}}) \end{cases} \quad (17)$$

Therein, R_{Hf} denotes the gas constant of hafnium vapour, P_{1atm} is the standard pressure, and T_{melt} is the melting temperature of Hf with $\Delta T = 0.1$ K.

The mass flux of re-deposition vapour Γ_{dep} was calculated as

$$m_{\text{Hf}} \Gamma_{\text{dep}} = m_{\text{Hf}} \frac{1}{4} \frac{\rho Y_{\text{Hf}}}{m_{\text{Hf}}} \sqrt{\frac{8kT_c}{\pi m_{\text{Hf}}}} = \rho Y_{\text{Hf}} \sqrt{\frac{kT_c}{2\pi m_{\text{Hf}}}}. \quad (18)$$

2.5. Thermodynamic and transport properties of solid material, transport properties of oxygen plasma and Hf vapour

Table 1 shows the thermodynamic properties of solid materials used in this work. The characteristics of Hf with the low specific heat, low thermal conductivity, high melting and boiling temperature, and with other features are compared with the characteristics of Cu.

Thermodynamic and transport properties of oxygen thermal plasma with hafnium vapour were calculated under the local thermodynamic equilibrium assumption. First, the equilibrium composition of oxygen, hafnium vapour at different pressure was calculated as a function of the temperature from 300 to 30 000 K by using minimization of Gibbs' free energy. The species included in the calculations were as follows: for oxygen, O_3 , O_2 , O_2^- , O_2^+ , O , O^+ , O^{2+} , and e ; for hafnium, Hf , Hf^+ , and e . Using the calculated equilibrium composition, we computed the thermodynamic properties like enthalpy h , specific heat C_p , and mass density ρ . Transport properties such as the electrical conductivity σ , the thermal conductivity λ , and the viscosity η were calculated based on the first-order approximation of the Chapman–Enskog method using the calculated equilibrium composition and collision integrals [15]–[20]. The collision integrals classified into momentum transfer cross section and viscosity cross section for interactions between oxygen species and hafnium species. The required collision integrals for interactions between oxygen species were calculated using the method given by [17, 20]. The collision integrals for Hf-Hf interactions were obtained by using exponential repulsive potential given by Abrahamson [21] and Monchick' table [22]. The collision integrals for Hf-Hf⁺ interactions were calculated considering the effects of resonant charge exchange [20], which is interpolated from the Rapp's data versus ionization potential [23]. For interactions of e-Hf, the collision integrals estimated by the hard-sphere method. In addition, the thermodynamic and transport properties for the mixture of hafnium vapour and oxygen were found by using a mixture law based on the concentration ratio. The resulting properties of the gas mixture were applied to thermo-fluid analysis as functions of temperature.

The effective diffusion coefficient of Hf vapour in oxygen D_{Hf-O_2} was calculated from the following effective binary diffusion coefficient approximation for simplicity [16, 19]:

$$D_{Hf-O_2} = \frac{3kT}{8p} \left[\frac{\pi kT(m_{O_2} + m_{Hf})}{2m_{O_2}m_{Hf}} \right]^{\frac{1}{2}} \frac{1}{Q_{Hf-O_2}} \quad (19)$$

where k is the Boltzmann constant, m_{O_2} is the mass of O_2 atom, m_{Hf} is the effective mass of Hf vapour depending on particle composition of Hf vapour, Q_{Hf-O_2} is the effective momentum transfer cross section between O_2 and Hf vapour, which was estimated from the hard-sphere method.

The radiation loss P_{rad} was computed while taking account of atomic and ionic spectral lines and the continuous spectrum including the bremsstrahlung and the

recombination radiation by using the following classical expressions [20]:

$$P_{\text{rad}} = \frac{4\pi}{(4\pi\epsilon_0)^3} \frac{16\pi e^6 n_e}{3c^3 (6\pi m_e^3 k T_e)^{\frac{1}{2}}} \frac{4kT_e}{h_p} + \sum_{\text{all-lines}} \frac{n_\ell}{4\pi Z_\ell} \frac{h_p c}{\lambda_\ell} g_\ell A_\ell \exp\left(-\frac{E_\ell}{kT_e}\right) \quad (20)$$

where c is the velocity of light, Z_ℓ is the partition function of speccies ℓ , n_ℓ the number density of speccies ℓ , h_p the Planck's constant, g_ℓ the statistical weigh, A_ℓ the transition probability, E_ℓ the energy of the upper level, λ_ℓ the wavelength. All data sources used in the calculation were taken from [24, 25, 26].

2.6. Boundary conditions

Figure 1 shows the computational domain where O-A-B-C-D-E-F-G-H-I-K-L define the calculation space inside which fluid parameters and scalar quantities were evaluated. The two-dimensional space coordinates are O (0, 0), A (0, 9.3), B (9.3, 0.67), C (9.3, 4.3), D (0, 4.3), E (0, 3.4), F (1.4, 2.7), G (1.4, 0.63), H (1.4, 0), I (3.8, 1.3), K (5.1, 1.3) and L (6.3, 0.67) where the unit is millimeters. The non-uniform grid system with a size of 98 nodes in the vertical direction and 185 nodes in the horizontal direction is applied to the analytic space. The non-slip condition was considered on all the boundary walls between solid and gas HG, GI, EI, and BD. On axis OA, the axial symmetry condition is applied. The following conditions were set at the boundary of the computational domain:

At the centre axis (OA):

$$\frac{\partial u}{\partial r} = 0; \quad v = 0; \quad \frac{\partial w}{\partial r} = 0; \quad \frac{\partial T}{\partial r} = 0. \quad (21)$$

At the copper wall (OE, DCB):

$$u = 0; \quad v = 0; \quad w = 0; \quad T = 300\text{K}. \quad (22)$$

At the outlet (AB):

$$\frac{\partial(\rho u)}{\partial z} = 0; \quad \frac{\partial(\rho v)}{\partial z} = 0; \quad \frac{\partial(\rho w)}{\partial z} = 0; \quad \frac{\partial T}{\partial z} = 0. \quad (23)$$

At the inlet (ED):

$$u = u_{\text{in}} \quad v = 0; \quad w = w_{\text{in}}; \quad T = 300\text{K}; \quad p = p_{\text{in}}. \quad (24)$$

Oxygen gas is injected from the inlet ED with a swirl component that can be expressed by the swirl gas angle [12].

In this paper, the calculation model is performed by the shape of cathode holder, as shown Figure 1. The cathode holder shape is defined a convex structure which protrudes from the surface of the cathode holder, as called "convex cathode holder". For purposes of studying the effects of cathode holder shape on the behaviour of hafnium cathode evaporation, figure 2 shows three cases of cathode holder shape are origin flat surface

holder and different protrusion of convex cathode holder, as called "h(o), h(a), h(b)", respectively.

In addition, the operating parameters for simulation are that the swirl gas angle is fixed at 15 deg. The arc current of 100 A and gas flow rate of 20 slm are fixed for this calculation model. Pressure is also fixed at 0.9 MPa. For simplicity, the boundary shape is assumed not to change by melting and evaporation. The SIMPLE method described by Patankar [27] was used for the calculation scheme to solve the governing equations described in the previous section.

3. Calculation Results

3.1. Effects of convex cathode holder on the arc plasma characteristics

Figure 3 portrays the temperature distributions of arc plasma with cathode holder shapes of h(o), h(a), and h(b). It is apparent that the arc root near the cathode is expanded in the radial direction with effect of convex cathode holder. The arc root motion will tend to move to surface of holder cathode with the higher protrusion of convex cathode holder.

The radial distribution of the surface temperature of the hafnium cathode for different cathode holder shapes is presented in Figure 4. The hafnium cathode surface temperature is decreased markedly in range of 0.4 mm with effect of convex cathode holder. The higher protrusion of convex cathode holder results in the lower hafnium surface temperature. This decrease in surface temperature is related mainly with arc motion by the changing of convex cathode holder, as described later. This rapid arc motion is expected to decrease the heat transferred to the surface cathode by the effect plasma gas flow. However, there is no significant change in the temperature of surface holder, which is remain lower than the melting temperature of copper even though the effect of convex cathode holder.

In addition, figure 5 and figure 6 show the radial distribution of arc plasma temperature and current density just near the cathode surface. These results suggest that the decreasing of arc plasma temperature and current density with effect convex cathode holder occur at the same radial position closer to the axis centre. An increase in protrusion of convex cathode holder induces the expansion of arc root resulting in a low current density in the immediate vicinity of the cathode, which decreases the efficient heating of cathode surface and therefore a descending in hafnium insert temperature.

Figure 7 depicts a comparison of gas flow fields obtained with the cathode holder shapes of h(o), h(a), and h(b). As a result described in flat surface holder h(0), the gas flow in front of surface cathode moves away from cathode by effect of swirling gas flow and hence improves the heat transfer to the gas at the cathode surface. This downstream gas flow from cathode is reduced markedly by convex cathode holder h(b). However, in the cathode holder h(c) case, it is noteworthy that a circular vortex appears in front of hafnium cathode in which the flow direction is mainly toward the cathode

and moves in the direction against that of the swirling gas flow. Figure 8 also shows the axial distribution of velocity along the center axis. It is indicated that the velocity has a negative its value in axial position close to cathode with convex cathode holder. This negative axial velocity shows a considerable rise with increase in protrusion of convex cathode holder.

Furthermore, the arc rotation velocity V_{rot} is simply calculated as following equation:

$$V_{rot} = [\nabla \times \mathbf{u}]_{\theta} = \frac{\partial u}{\partial z} - \frac{\partial v}{\partial r}. \quad (25)$$

Figure 9 presents the arc rotation velocity distribution with different cathode holder shapes. In case of flat surface holder h(0), the high counter-clockwise arc rotation near the center axis occurs at nozzle throat region, resulting in high constricted arc plasma and quality of speed cutting. However, it appears a clockwise arc rotation in the vicinity of hafnium cathode with convex cathode holder, corresponding with the rotating direction of the gas flow vortex. The acceleration of the clockwise rotation of gas velocity is more evident in case of cathode holder h(b).

Thus, calculations showed that the convex holder cathode not only reduces the gas flow velocity from cathode surface, but also makes a vortex in vicinity of cathode surface moving in the opposite direction. The magnitude of vortex is reflected by the arc rotation velocity. Therefore, the arc root moves more onto the holder cathode region. On the other hand, the rapid clockwise rotation velocity against the effect of swirling gas flow from cathode is expected to provide more convective cooling of hafnium cathode surface, resulting in decreasing of cathode surface temperature. The presence of this vortex can be related to the evaporation amount of hafnium cathode which is discussed in next section.

3.2. Effects of convex cathode holder on evaporation amount of hafnium cathode

Figure 10(a) and (b) show the distributions of the mass fraction of hafnium vapour with consideration of redeposition and without that of redeposition for different cathode holder shapes. Results demonstrated that the mass fraction of hafnium vapour with convex cathode holder decreases markedly in comparison with flat holder h(o). This is because the current density, and therefore the cathode surface temperature, is lower. The consideration of redeposition of hafnium vapour reduces the mass fraction of hafnium vapour in three cases of cathode holder shape.

The results from cathode holder shape of h(o) and h(a) show that the high hafnium vapour is concentrated in the high radial current density near the cathode surface and transported to the downstream region of the plasma torch along the centre axis by convection. In case of holder h(b), as significant effect of convex cathode holder, the hafnium vapour spreads out a larger area near cathode surface, according to the arc root motion by gas flow vortex. Moreover, the hafnium vapour without consideration of redeposition covers the entire surface of hafnium cathode by higher concentration of hafnium vapour.

As described in this paper, the net evaporation mass flux $m_{\text{Hf}}\Gamma_{\text{net}}$ [kg/(m²s)] can be estimated as

$$m_{\text{Hf}}\Gamma_{\text{net}} = m_{\text{Hf}}(\Gamma_{\text{evp}} - \Gamma_{\text{dep}}). \quad (26)$$

The mass flux of hafnium vapour ejected from the cathode for different cathode shapes are given in figure 11. Comparison of net evaporation mass flux between convex the cathode holder and flat cathode holder h(o) indicated that the net mass flux effect of convex holder has a decrease markedly in the entire hafnium cathode surface. The appearance of the negative net evaporation flux around the arc fringe in vicinity of hafnium cathode is dominated by the evaporated atoms returning to cathode surface.

In addition, the mass loss attributable to evaporation of the hafnium cathode was estimated from these results obtained using the following equation:

$$M_{\text{Hf}} = \int_0^{\infty} m_{\text{Hf}}(\Gamma_{\text{evp}} - \Gamma_{\text{dep}})2\pi r dr. \quad (27)$$

Figure 12 shows the calculated total amount of mass loss of the hafnium cathode different cathode shapes comparing with no redeposition of hafnium vapour. Showing the same trend as that of the mass flux of hafnium vapour, the effect of convex holder cathode reduces the amount of mass loss of hafnium cathode evaporation. The higher protrusion of convex cathode holder induces the lower amount of mass loss even this progress decreases slowly in comparison of convex cathode holder h(a) and h(b). The reason for a decrease in amount of mass loss is that the presence of gas flow vortex close to the cathode surface moves in the clockwise direction. This gas flow vortex motion toward to hafnium cathode reduces the probability of evaporated hafnium escaping from cathode surface and also facilitates the evaporated atoms returning to cathode surface. In addition, as shown in this figure, the redeposition of hafnium vapour decreases the mass loss of the hafnium cathode.

4. Conclusions

Results of numerical simulations of the influence of cathode holder shape on hafnium cathode evaporation for oxygen plasma cutting arc torch are described in this paper. We have developed a two-dimensional thermofluid model for plasma cutting arcs with different convex cathode holders.

The simulated results show that the convex holder cathode not only reduces the gas flow velocity from cathode surface, but also makes a vortex in vicinity of cathode surface moving in the opposite direction. The cathode surface temperature decreases markedly with the higher protrusion of convex cathode holder resulted in a rapid clockwise rotation of gas flow velocity.

In addition, the presence of gas flow vortex toward to cathode surface reduces the probability of evaporated hafnium escaping from cathode surface and also facilitates the evaporated atoms returning to cathode surface. Thus, the mass flux and total amount of mass loss of hafnium cathode were predicted to decreases significantly with effect of convex cathode holder.

References

- [1] Nemchinsky V A, and Severance W S 2006 What we know and what we do not know about plasma arc cutting *J. Phys. D: Appl. Phys.* **39** R423-8.
- [2] Colombo V, Concetti A, Ghedini E, Dallavalle S, and Vancini M 2009 High-speed imaging in plasma arc cutting: a review and new developments *Plasma Sources Sci. Technol.* **18** 023001.
- [3] Peters J, Yin F, Borges C F M, Heberlein J, and Hackett C 2005 Erosion mechanisms of hafnium cathodes at high current *J. Phys. D: Appl. Phys.* **38** 1781-94.
- [4] Luo L et al 1997 Electrode for a plasma arc torch *Hypertherm Inc. Patent* US 5,601,734.
- [5] Sakyragi S 1193 Cathod structure of plasma arc torch *Kabushibi Kaishia Komatsu. Patent* US 5,177,338.
- [6] Peters J, Bartlett B, Lindsay J, and Heberlein J 2008 Relating spectroscopic measurements in a plasma cutting torch to cutting performance *Plasma Chem Plasma Process* **28** 331-352.
- [7] Colombo V, Concetti A, Ghedini E, and Nemchinsky V 2010 High-speed imaging investigation of transition phenomena in the pilot arc phase in Hf cathodes for plasma arc cutting *Plasma Sources Sci. Technol.* **19** 065025.
- [8] Colombo V, Concetti A, Ghedini E, Rotundo F, Sanibondi P, Boselli M, Dallavalle S, Gherardi M, Nemchinsky V, and Vancini M 2010 Advances in plasma arc cutting technology: The experimental part of an integrated approach *Plasma Sources Sci. Technol.* **19** 065025.
- [9] Nemchinsky V A, and Showalter M S 2003 Cathode erosion in high-current high-pressure arc *J. Phys. D: Appl. Phys.* **36** 704-12.
- [10] Nemchinsky V A 2002 Cathode erosion rate in high-pressure arcs. Influence of swirling gas flow *IEEE Trans. Plasma Sci.* **30** 2113-6.
- [11] Zhou Q, Yin H, Lin H, Xu X, Liu F, Guo S, Chang X, Guo W, and Xu P 2009 The effect of plasma-gas swirl flow on a highly constricted plasma cutting arc *J. Phys. D: Appl. Phys.* **42** 095208.
- [12] Nguyen Phi Long, Tanaka Y, and Uesugi Y 2012 Numerical investigation of the swirl gas angle and arc current dependence on evaporation of hafnium cathode in a plasma cutting arc *IEEE Trans. Plasma Sci.* **40** no. 2, 497-504.
- [13] Nguyen Phi Long, Katada Y, Tanaka Y, Uesugi Y and Yamaguchi Y 2012 Cathode diameter and operating parameter effects on hafnium cathode evaporation for oxygen plasma cutting arc *J. Phys. D: Appl. Phys.* **45** 435203 (14pp).
- [14] Boulos M I, Fauchais P, and Pfender E 1994 Thermal plasmas fundamentals and applications. Vol. I. Plenum Press.
- [15] Tanaka Y, Yamachi N, Matsumoto S, Kaneko S, Okabe S and Shibuya M 2008 Thermodynamic and Transport Properties of CO₂, CO₂-O₂ and CO₂-H₂ Mixtures at Temperatures of 300–30,000K and at Pressures of 0.1–10 MPa *Electrical Engineering in Japan*, **163-4** 18-29.
- [16] Murphy A B 2001 Thermal plasmas in gas mixtures *J. Phys. D: Appl. Phys.* **vol. 34** R151–R173.
- [17] Murphy A B and Arundell C J 1994 Transport coefficients of argon, nitrogen, oxygen, argon-nitrogen, and argon-oxygen plasma *Plasma Chem. Plasma Process.* **14** 451-90.
- [18] Tanaka Y 2004 Two-temperature chemically non-equilibrium modelling of high-power ArN₂ inductively coupled plasma at atmospheric pressure *J. Phys. D: Appl. Phys.* **37** 1190205.
- [19] Murphy A B 2010 The effects of metal vapour in arc welding *J. Phys. D: Appl. Phys.* **vol. 43** 434001.
- [20] Yos J M 1963 Transport properties of nitrogen, hydrogen, oxygen and air to 30,000 K *Technical Memorandum* RAD-TM-63-7 AVCO Corporation
- [21] Abrahamson A A 1969 Born-Mayr-type interatomic potential for neutral ground-state atoms with Z=2 to Z=105 *Phys. Rev.* **178** 76-79.
- [22] Monchick L 1959 Collision integrals for the exponential repulsive potential *Phys. Fluids* **2** 695-700.
- [23] Rapp. D and Francis W E 1962 Charge exchange between gaseous ions and atoms *J. Chem. Phys.* **37** 2613-2645.

- [24] Charles H C and William R B, Experimental transition probabilities for spectral line of seventy elements, National Bureau of Standards Monograph 53, July, 1962.
- [25] NIST Atomic Spectra Database, National Institute of Standards and Technology, <http://www.nist.gov/>.
- [26] M.W. Chase, Jr. et al., NIST-JANAF Thermochemical Tables, Fourth edition, *J. Phys. Chem. Ref. Data*, Monograph 9, 1998.
- [27] Patankar S V 1980 Numerical Heat Transfer and Fluid Flow Hemisphere Pub. Corp. New York

Table 1. Thermodynamic properties of the solid material.

Solid	ρ_s [kg/m ³]	C_{ps} [J/kg/K]	λ_s [W/m·K]	T_{melt} [K]	T_{boil} [K]	L_m [MJ/kg]	L_v [MJ/kg]	W_ℓ [eV]
Cu	8930	385.62	381	1356	2855	0.206	4.815	4.65
Hf	13310	140	23	2506	4876	0.1347	3.211	3.53

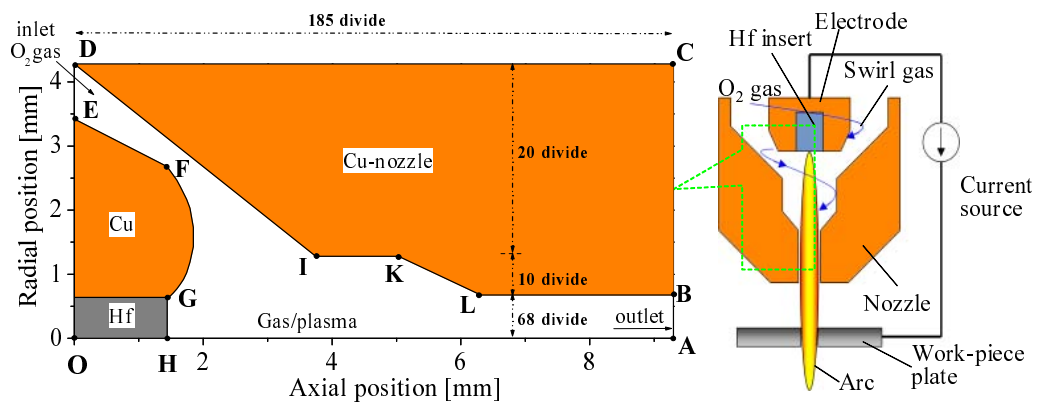


Figure 1. Schematic diagram of plasma cutting torch

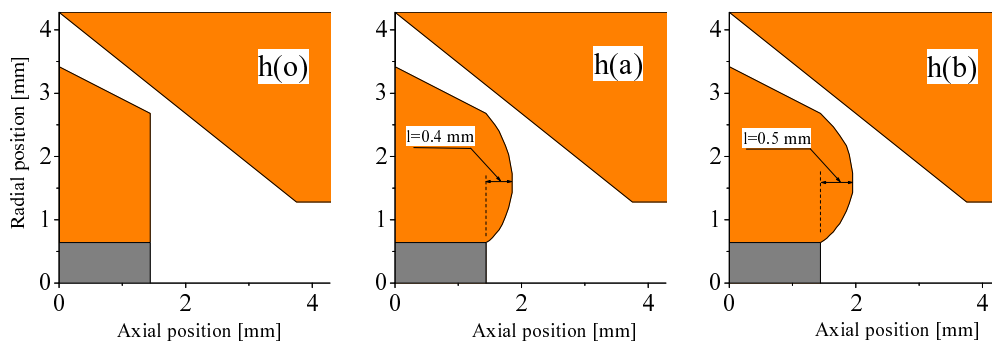


Figure 2. The shape of cathode holder.

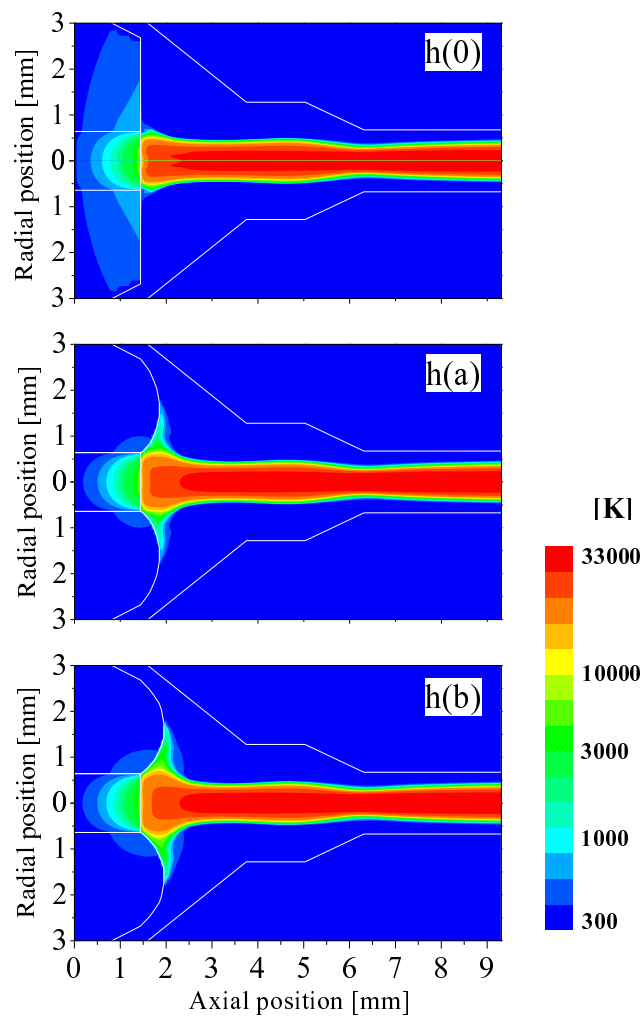


Figure 3. Temperature distribution of arc plasma with different cathode holder shapes.

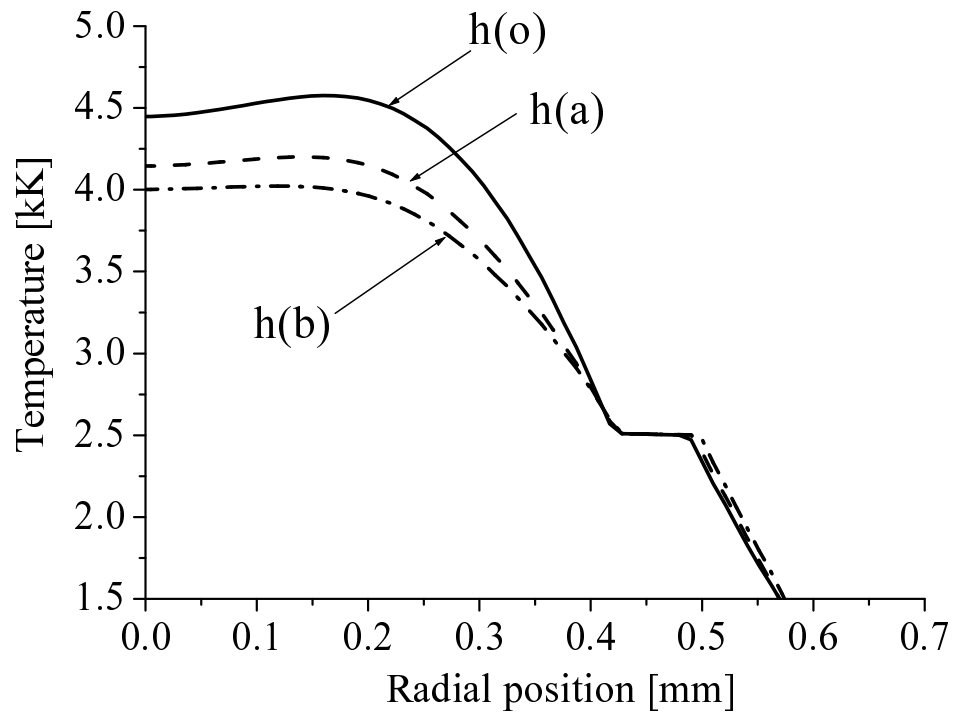


Figure 4. Radial distributions of the Hf cathode surface temperature for different cathode holder shapes.

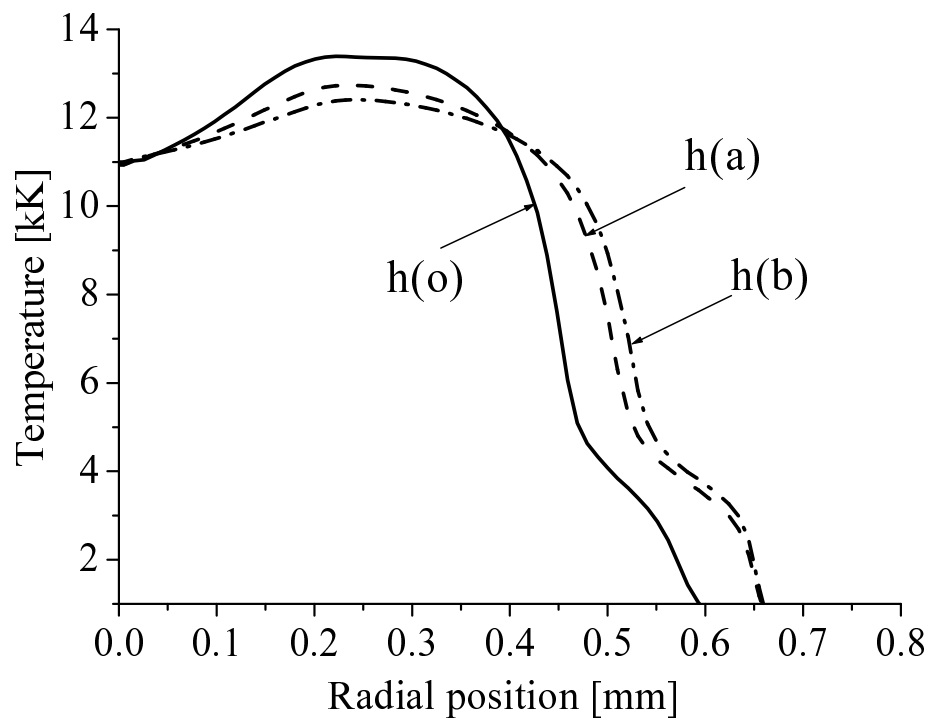


Figure 5. Radial distributions of the arc plasma temperature near the cathode surface for different cathode holder shapes.

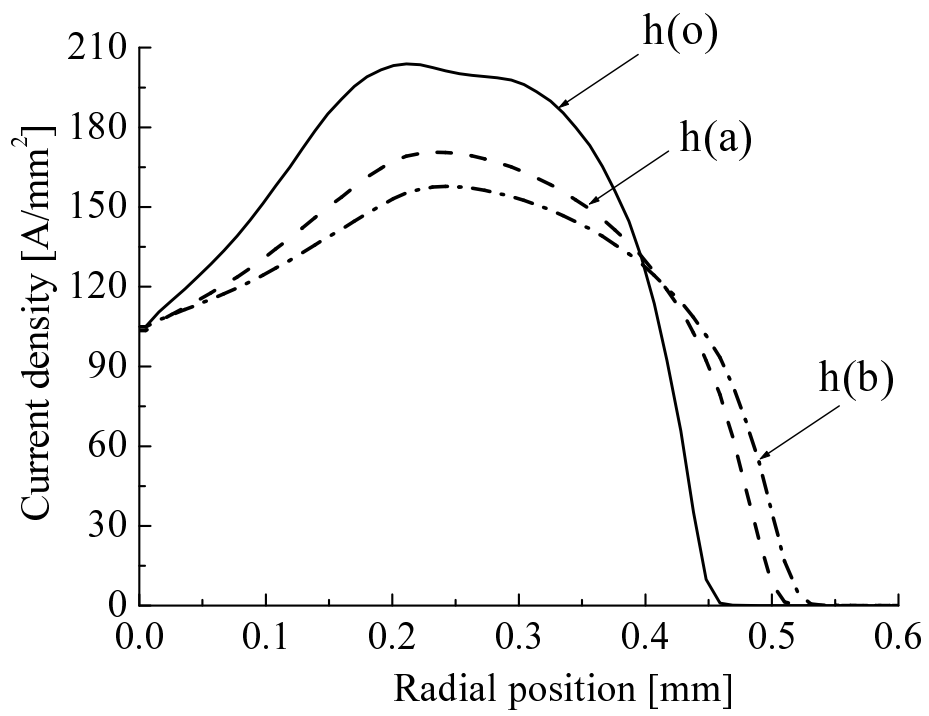


Figure 6. Radial distributions of current density near the cathode surface for different cathode holder shapes.

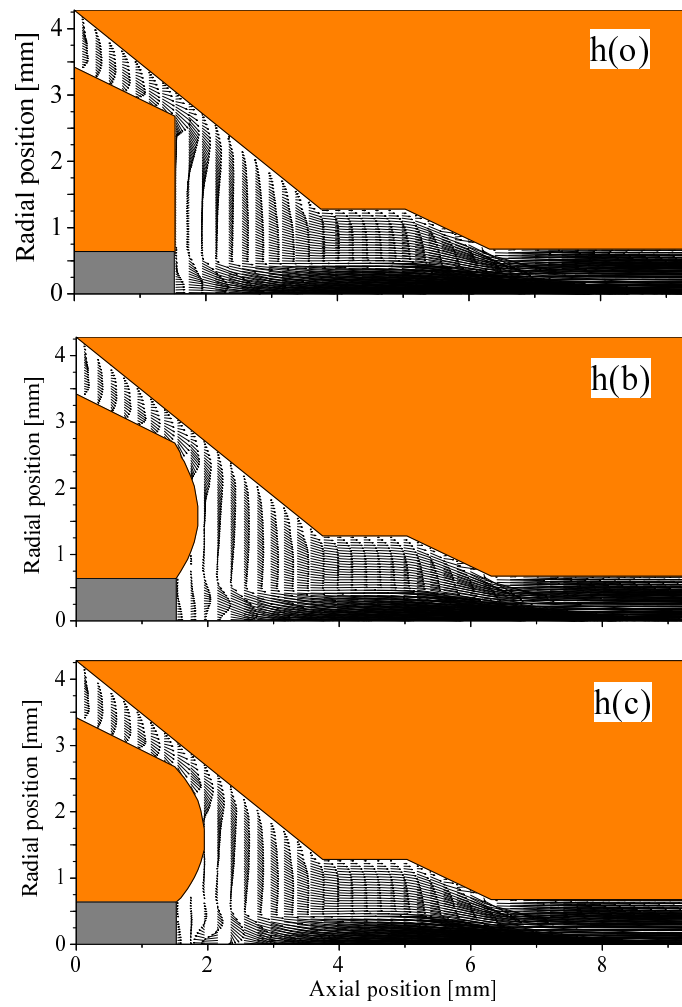


Figure 7. Gas flow fields with different cathode holder shapes.

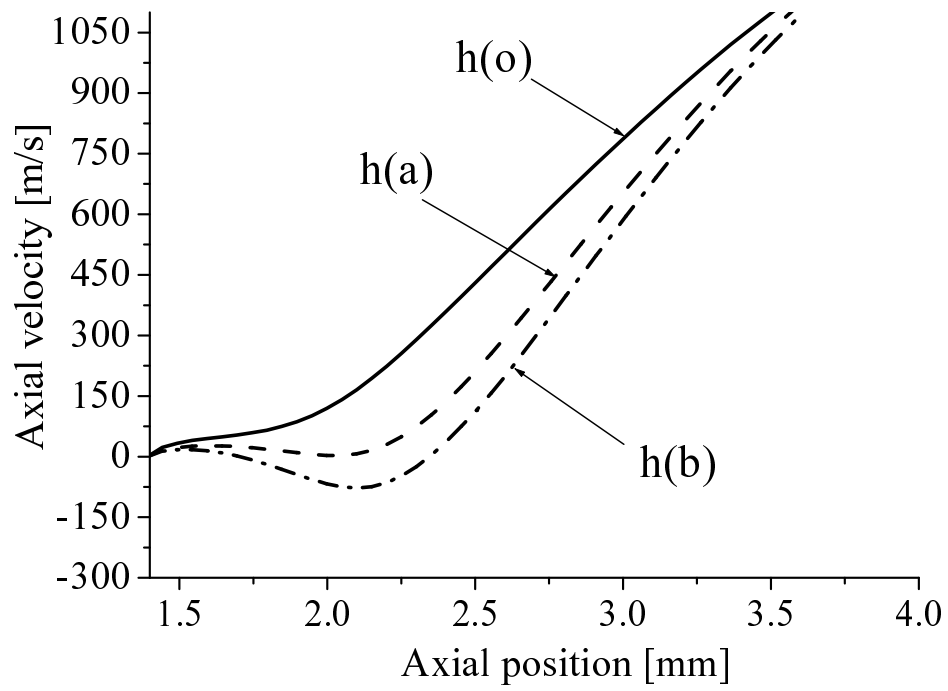


Figure 8. Axial distributions of velocity along the center axis for different cathode holder shapes.

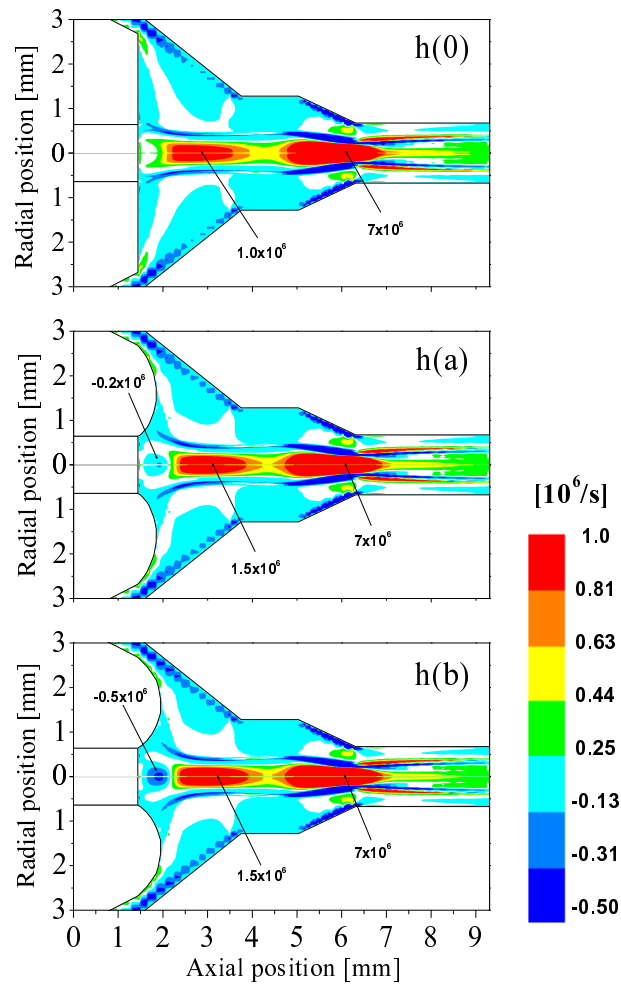


Figure 9. Distributions of arc rotation velocity with different cathode holder shapes.

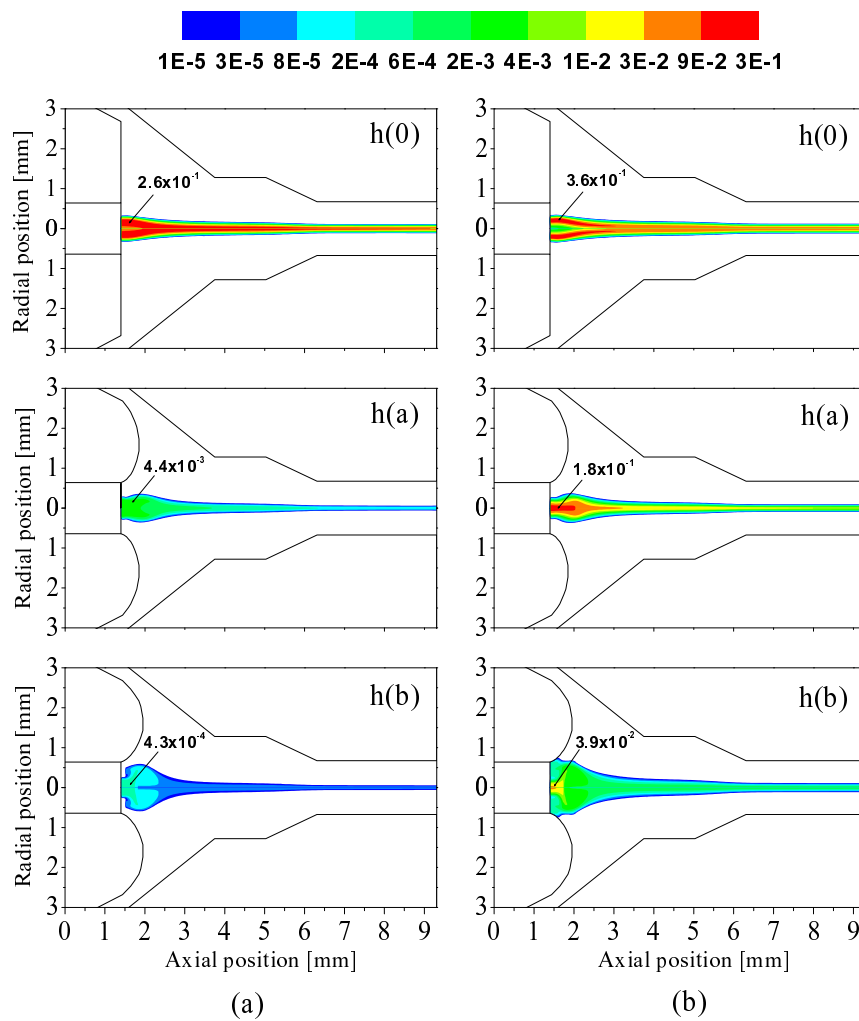


Figure 10. Distributions of mass fraction of Hf vapour with different cathode holder shapes: (a) with redeposition; (b) without redeposition.

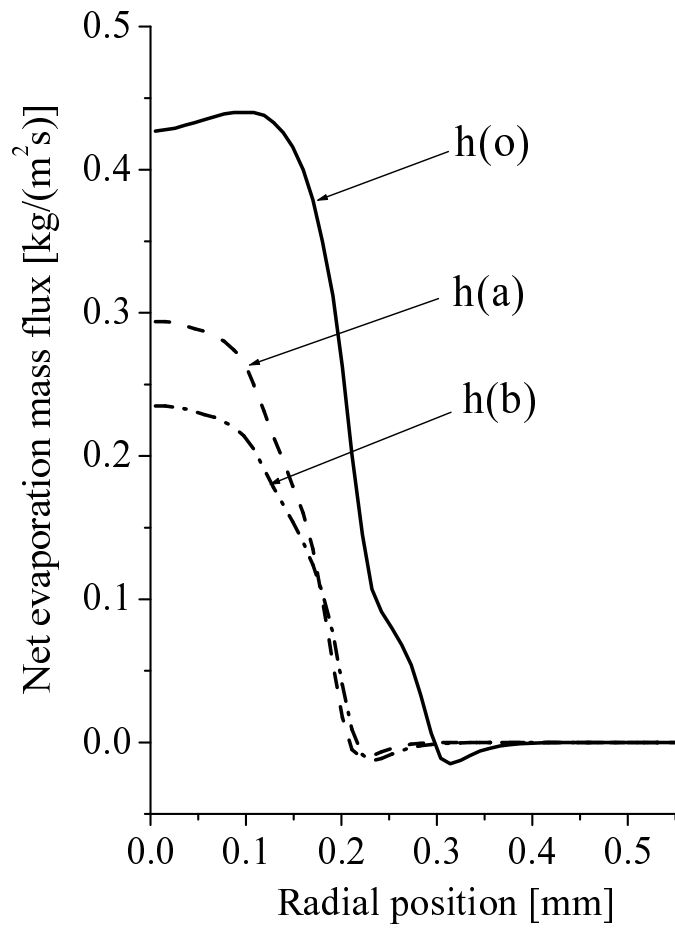


Figure 11. Radial distributions of net evaporated mass flux from Hf cathode for different cathode holder shapes.

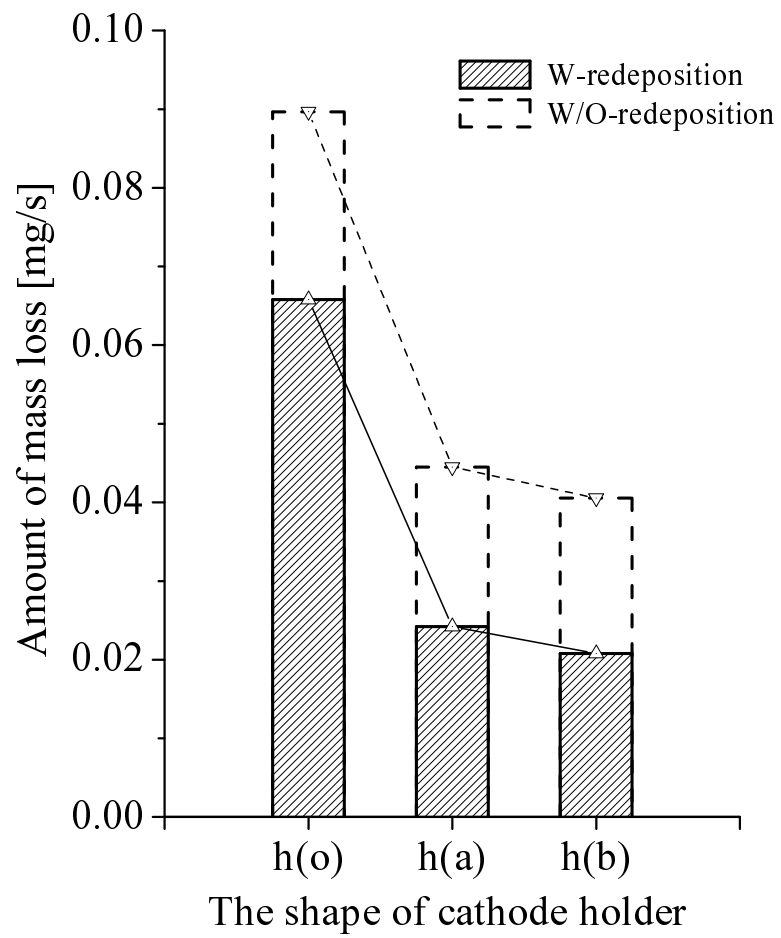


Figure 12. amounts of mass loss of Hf cathode evaporation for different cathode holder shapes.